INSTITUTE OF PHYSICS PUBLISHING JOURNAL OF OPTICS B: QUANTUM AND SEMICLASSICAL OPTICS

J. Opt. B: Quantum Semiclass. Opt. **6** (2004) 135–142 PII: S1464-4266(04)66846-7

Broadening mechanisms and their effects in non-classical correlations on cavity QED with atomic beams

J E Reiner, F M Dimler and L A Orozco[1]

Department of Physics and Astronomy, State University of New York, Stony Brook, NY 11794-3800, USA

E-mail: Lorozco@UMD.EDU

Received 31 July 2003, accepted for publication 26 November 2003
Published 3 February 2004
Online at stacks.iop.org/JOptB/6/135 (DOI: 10.1088/1464-4266/6/2/003)

Abstract
Doppler and transit broadening effects inherent in a thermal atomic beam reduce the size of quantum fluctuations in a cavity QED system. A cold continuous atomic beam would reduce these effects, but would not eliminate the different atom–field couplings associated with the random distribution of atoms throughout the cavity. We present results that describe the effect that this has on quantum fluctuations and how it could be used to improve future studies on the fluctuations from a cavity QED system. We also report on experimental progress towards a continuous cold atom source.

Keywords: cavity QED, non-classical states, intensity correlations

1. Introduction

The steady-state photon occupation number for a strongly coupled system in the weak driving limit is much less than one. In this limit, the emission of a single photon initiates fluctuations that have been shown to violate classical inequalities. The detection of the photon informs the experimenter that a large fluctuation is underway, and using the condition that a measurement is taken on photon arrival allows one to observe the quantum dynamics of the system. Single-photon fluctuations have been observed with conditional intensity [1] and conditional field [2] measurements.

We consider the many-atom optical cavity QED system with N two-level atoms coupled to a single TEM_{00} mode of a Fabry–Perot cavity. When the atoms have been injected into the cavity with a thermal beam, Doppler and transit broadening effects typically degrade the size of the quantum fluctuations by more than 50% [3, 4]. Cold atomic beams [5] extracted from a magneto-optical trap could overcome these broadening effects, but it would still create a random distribution of atom–field couplings throughout the cavity mode. A single atom held in a trap in a cavity [6–10] may even be subject to broadening from the harmonic energy levels of the trap that smear out the dipole coupling of the atom to the field [11].

In order to better observe the quantum effects associated with the conditioned fluctuations, we would like to further understand the influence that the beam has on the size of the fluctuations. Previous efforts have used numerical calculations [1, 3]. In this paper, we present a solution to the problem of a set of randomly distributed atoms coupled to a Gaussian TEM_{00} mode of the cavity based on the distribution of atoms in the cavity mode. This result is used to discuss the limitations that a slow atomic beam creates in the observation of quantum effects.

The extraction of cold atoms from a magneto-optic trap (MOT) is an avenue for future experiments in cavity QED. There are different geometries and realizations in developing such beams. (The following reviews point to relevant experiments [12–14].) Our experiment requires a continuous beam of atoms in order to reduce atomic number fluctuations and there should be no overlapping light fields that disturb the coupling of the atoms to the cavity.

The paper is organized as follows: section 2 introduces the cavity QED system and two types of correlation measurements that illuminate the conditional dynamics. Section 3 details the calculation of the conditional dynamics with an atomic beam and includes a comparison of the theory and past experiments.

[1] Present address: Department of Physics, University of Maryland, College Park, MD 20742-4111, USA.

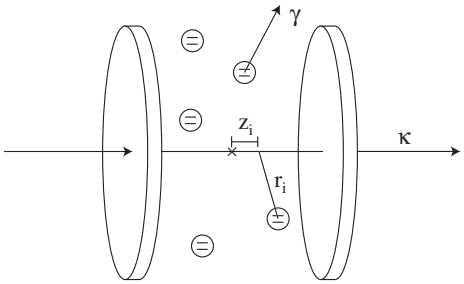

Figure 1. The many-atom cavity QED system. The coupling of the ith atom is parametrized by its position in the cavity. The system radiates through spontaneous emissions and cavity emissions.

Section 4 presents our experimental setup for a cold atomic beam and section 5 is the conclusion.

2. Theory

2.1. Cavity QED system

The many-atom cavity QED system [15] consists of N two-level atoms, randomly coupled to a single mode of a Fabry–Perot cavity, characterized by a field lowering (raising) operator $a(a^\dagger)$. The maximum atom–field coupling is parametrized by g

$$g = \mu\sqrt{\frac{\omega_a}{2\hbar\epsilon_0 V}} \tag{1}$$

where μ is the electric dipole moment of the two-level transition and V is the cavity mode volume. Transitions between the ground and excited states of the ith atom are described by the standard raising (lowering) Pauli spin operators $\sigma_i^\dagger$ (σ_i) and $\sigma_i^z = [\sigma_i^\dagger, \sigma_i]$. The Tavis–Cummings Hamiltonian describes the atom–field couplings and under the rotating wave approximation it is given by

$$H_{\mathrm{TC}} = \mathrm{i}\hbar\sum_i g_i(a^\dagger\sigma_i - a\sigma_i^\dagger) \tag{2}$$

where g_i is the strength of the coupling between the cavity and the ith atom. For a Gaussian TEM_{00} cavity mode the coupling is defined by

$$g_i(r, z) = g\cos(kz_i)\exp(-r_i^2/w^2) \tag{3}$$

where r is the radial distance from the cavity axis defined by z, k is the magnitude of the cavity field wavevector, and w is the cavity mode waist (see figure 1).

We assume throughout this paper that the atoms and cavity are on-resonance with each other and the driving field $\mathcal{E}$ described by

$$H_{\mathrm{d}} = \mathrm{i}\hbar(\mathcal{E}\mathrm{e}^{-\mathrm{i}\omega_0 t}a^\dagger - \mathcal{E}^*\mathrm{e}^{\mathrm{i}\omega_0 t}a). \tag{4}$$

We also assume that the cavity QED system is weakly and homogeneously coupled to the environment. This weak coupling allows for the Born–Markov approximation which traces out the environmental degrees of freedom and leaves a modified equation that describes the dynamics of the system alone. The result is a quantum master equation of the Lindblad form [16]

$$\begin{aligned}\dot\rho &= \mathcal{L}\rho \\ &= \frac{1}{\mathrm{i}\hbar}[H_{\mathrm{TC}} + H_{\mathrm{d}}, \rho] + 2\kappa\mathcal{D}[a]\rho + \sum_i \gamma_i\mathcal{D}[\sigma_i]\rho\end{aligned} \tag{5}$$

where $\mathcal{D}[A]B = ABA^\dagger - \frac{1}{2}(A^\dagger AB - BA^\dagger A)$ and both atom and cavity fields decay at rates $\gamma/2$ and κ respectively.

The influence that an atom has on the system is parametrized by the single-atom cooperativity parameter of the ith atom: $C_i = g_i^2/\gamma\kappa$ and the collective cooperativity parameter $C = \sum_i C_i$ that in the case of N maximally coupled atoms is: $C = NC_1$. Both relate the strength of the atom–field coupling to the two decay rates.

Figure 1 illustrates the model we use to describe the randomly coupled atoms in the cavity. The individual atoms spontaneously emit, so the atomic polarization radiatively decays at the rate $\gamma/2$ with the atomic inversion decaying at the rate γ and the cavity field leaks out at the rate κ.

2.2. Conditional dynamics

Multi-time correlation functions can be calculated from equation (5) in a deterministic manner, but quantum trajectories further illustrate the system dynamics by unravelling equation (5) in a way that corresponds to experimental measurements. Carmichael showed that, in the Markovian limit, equation (5) could be solved by a stochastic evolution of a wavefunction [16]. The stochastic nature of this evolution is directly related to the random nature of the photoemissions from the cavity QED system. A more complete discussion of quantum trajectories in relation to optical cavity QED can be found in [17]. In the weak field limit, with identical couplings, $g_i = g$, and assuming that $g\sqrt{N} > \kappa, \gamma$ the system wavefunction evolves into the following steady state [18]:

$$\begin{aligned}|\psi_{\mathrm{ss}}\rangle = |0, \mathrm{G}\rangle + \lambda\left(|1, \mathrm{G}\rangle - \frac{2g\sqrt{N}}{\gamma}|0, \mathrm{E}\rangle\right) \\ + \lambda^2\left(\xi_0\frac{1}{\sqrt{2}}|2, \mathrm{G}\rangle - \theta_0\frac{2g\sqrt{N}}{\gamma}|1, \mathrm{E}\rangle\right) + \cdots\end{aligned} \tag{6}$$

where $|n, \mathrm{G}\rangle$ describes the state with n photons in the cavity mode and all atoms in the ground state. We have not written the second order term in λ that represents two excitations in the atoms and none in the field, as we have limited our discussion to processes measurable by photons escaping out of the cavity and this term does not contribute. The $|\mathrm{E}\rangle$ state is the symmetrized one-atom excited state. λ is the steady-state field equal to $(\mathcal{E}/\kappa)/(1 + 2C)$, and

$$\begin{aligned}\xi_0 &= \frac{(1 - 2C_1')(1 + 2C)}{1 + 2C - 2C_1'} \\ \theta_0 &= \frac{1 + 2C}{1 + 2C - 2C_1'},\end{aligned} \tag{7}$$

where $C_1' = C_1[1/(1 + \gamma/2\kappa)]$ and ξ_0, θ_0 are of order unity for $C > C_1$, our regime of interest.

A cavity emission is modelled by acting with the cavity lowering operator, $\hat a$, on the steady state which results in the following dynamic wavefunction.

$$|\psi_c\rangle = |0, G\rangle + \lambda\left(\xi(\tau)|1, G\rangle - \theta(\tau)\frac{2g\sqrt{N}}{\gamma}|0, E\rangle\right) \quad (8)$$

where the conditioned field, $\xi(\tau)$, and the conditioned atomic polarization, $\theta(\tau)$, are both of the general form $f(\tau) = 1 + A_f \exp(-(2\kappa + \gamma)\tau/4)[\cos(\Omega\tau) + B_f \sin(\Omega\tau)]$ with A_f and B_f given by

$$A_\xi = \frac{-4CC_1'}{1 + 2C - 2C_1'} \quad (9)$$

$$B_\xi = \frac{2\kappa + \gamma}{4\Omega} \quad (10)$$

$$A_\theta = -\frac{A_\xi}{2C} \quad (11)$$

$$B_\theta = \frac{4\kappa^2 - \gamma^2 - 16\Omega^2}{16\Omega\kappa}, \quad (12)$$

where the vacuum Rabi frequency $\Omega = \sqrt{g^2N - ((\kappa - \gamma/2)/2)^2}$.

Note that the emission of a single cavity photon at time $\tau = 0$ causes a jump in both the cavity field and the atomic polarization of sizes A_ξ and A_θ respectively.

2.2.1. Classical bounds on the intensity correlation. The normalized two-time intensity correlation function is defined by

$$g^{(2)}(\tau) = \frac{\langle :I(t)I(t+\tau):\rangle}{\langle I(t)\rangle^2}. \quad (13)$$

By normal- and time-ordering the creation and annihilation operators of the intensity ($I = a^\dagger a$), and assuming the stationary state approximation, $g^{(2)}(\tau)$ can be considered a conditional intensity measurement. It gives the probability of detecting a photon at some delay τ following an initial photon. From equation (8) it is clear that this is equivalent to measuring $|\xi(\tau)|^2$. The quantum nature of the collapse of equation (6) makes it possible for the weakly driven cavity QED system to violate Schwarz type inequalities for $g^{(2)}(\tau)$. The two inequalities are

$$g^{(2)}(0) \geqslant 1 \quad (14)$$

$$|g^{(2)}(0) - 1| \geqslant |g^{(2)}(\tau) - 1|. \quad (15)$$

Carmichael *et al* [18] found an expression for the two-time intensity correlation in the weakly driven many-atom cavity QED system, for the case when the vacuum Rabi frequency (Ω) is real: $g\sqrt{N} > (\kappa - \gamma/2)/2$. Equation (16) shows $g^{(2)}(\tau)$ in terms of the coefficients associated with the field and polarization jumps from equations (8)–(10):

$$g^{(2)}(\tau) = |\xi(\tau)|^2 = |1 + A_\xi \exp[-(2\kappa + \gamma)\tau/4][\cos(\Omega\tau) + B_\xi \sin(\Omega\tau)]|^2, \quad (16)$$

A_ξ is the ratio of the change in the field to the mean field given that a photon is emitted. On resonance and for strong coupling, this change will always be negative. As the coupling constant g increases, C_1 increases and so does the size of the discontinuity, which grows relative to the steady-state amplitude λ. For very large coupling constants (large C_1), the jump can be many times larger than the mean intracavity field λ.

Figure 2 illustrates how the quantum jump associated with the cavity emission could lead to violations of equations (14) and (15). The size of the jump is given by $A_\xi(0) = 1 - \xi(0)$ and the correlation function equation (16) is determined at equal times by $\xi(0)$. So two ranges of values are possible: first if $0 < \xi(0) < 1$ we see a violation of equation (14). Second, if $\xi(0) < 0$ then there can be a violation of equation (15) without violating equation (14) [18]. This latter situation arises because the correlation function measures a conditional intensity, the conditional field is very negative and its square positive. This gives rise also to the phenomenon of 'bouncing' where the system oscillates at twice the vacuum Rabi frequency because of equation (16).

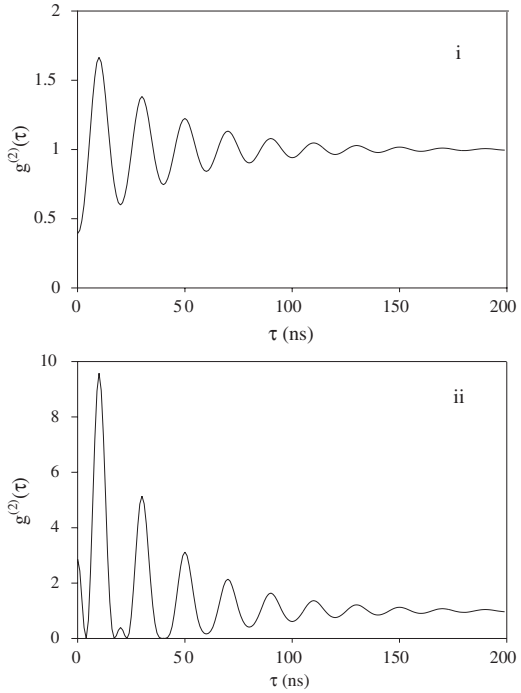

Figure 2. $g^{(2)}(\tau)$ for $(\kappa, \gamma, \Omega)/2\pi = (5, 6, 50)$ MHz and different atom–cavity coupling strengths. (i) Illustrates a violation of equation (14) for $g/2\pi = 3$ MHz and (ii) shows a violation of equation (15) for $g/2\pi = 8$ MHz. Notice the function 'bouncing' off the zero axis that corresponds to the field crossing zero.

2.2.2. Atomic polarization–intensity cross-correlation. The quantum phenomenon in the dynamics is the presence of the jump in the cavity field following the photoemission. Looking back at equation (6) one can see that this jump depends on ξ_0 which modifies the $|2, G\rangle$ amplitude away from the coherent state value of 1. This is due to the atom–field coupling, g, and the jump is evidence of the non-classical nature of the cavity field.

Equation (5) can be used to derive a set of Maxwell–Bloch equations that describe the dynamics of the expectation values for the cavity and atomic degrees of freedom (see for example [19]). Fluctuations in the cavity field can be initiated with a step in the drive at some time $\tau = 0$. It is important to note that although the cavity field will experience a jump at $\tau = 0$, the polarization field will not. The polarization field will simply lag behind the cavity field in its oscillation. Evidence for the true nature of the entanglement of this system lies in observing the jump in the polarization field following

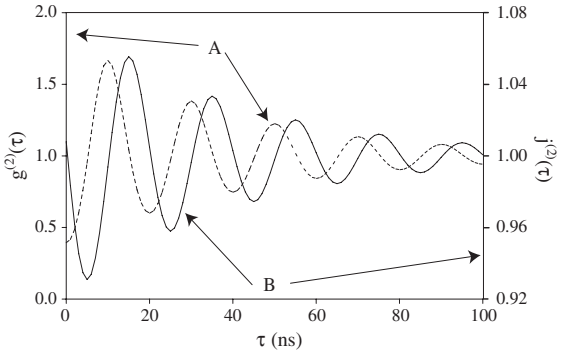

Figure 3. Intensity–intensity correlation $g^{(2)}(\tau)$ (dashed curve A) and atomic polarization–intensity cross-correlation $j^{(2)}(\tau)$ (continuous curve B) comparison for cavity QED $(\kappa, \gamma, g, \Omega)/2\pi = (5, 6, 3, 50)$ MHz. Notice the difference in scales between the two correlation functions.

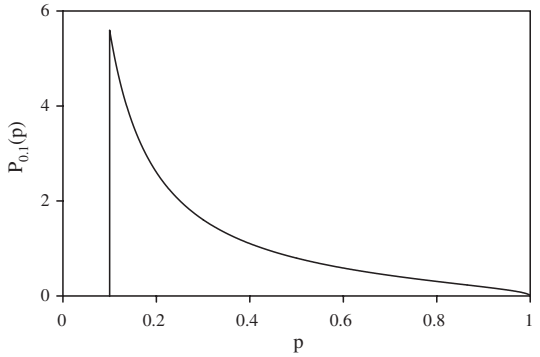

Figure 4. The one-atom probability distribution for the coupling to the cavity with $F = 0.1$.

an emission along the cavity axis. The following correlation function should be used to observe such a jump:

$$j^{(2)}(\tau) = \frac{\langle a^\dagger \sigma^\dagger(\tau)\sigma(\tau)a\rangle}{\langle \sigma^\dagger\sigma\rangle\langle a^\dagger a\rangle}. \tag{17}$$

$j^{(2)}(0)$ quantifies the degree of entanglement in the jump. This correlation function is difficult to measure in general, but in the weak field limit we can resort to the conditional measurements discussed before and condition a fluorescence intensity measurement on the detection of a cavity photon. From equation (8) we find that $j^{(2)}(\tau)$ is equivalent to $|\theta(\tau)|^2$ and that the size of the step in the fluctuation is given by $|1 + A_\theta|^2$. Denisov *et al* have studied this correlation function and its time reversal properties in [20].

Figure 3 compares the quantum jump associated with the cavity emission between the cavity field and the polarization field. Notice both the step in the polarization field at $\tau = 0$ and the difference between the two fluctuations.

3. Calculation of conditional dynamics with an atomic beam

In order to observe violations of equation (15) shown in figure 2(ii) and to see the step in the polarization field in figure 3, we need to optimize the size of the field step A_ξ. This can be accomplished with a large atom–field coupling g and a continuous cold atom beam which should reduce broadening effects. For the case of N identically coupled atoms equation (9) reduces, in the limit of large N, to $A_\xi = 1 - 2C_1'$. This means that removing broadening effects should allow us to observe bouncing when $C_1' = 1/2$. This result does not take into account the random distribution of the atoms throughout the cavity. In this section we present an analytical approach that describes the random distribution of the atoms along with homogeneous transit broadening effects and a comparison of these two modifications with recent experimental results.

3.1. Calculation

Carmichael and Sanders [21] showed that the one-atom probability distribution for a standing wave TEM_{00} cavity mode is

$$P_F(p) = \vartheta_F \frac{\cos^{-1}(p)}{p}\,\mathrm{d}p, \tag{18}$$

where p is the ratio $g(x, y, z)/g$, ϑ_F is the normalization constant of the distribution, and F is the normalized interaction volume inside which $p \geqslant F$. We ignore any atoms with $g_i < gF$. Figure 4 shows the features of this distribution. Notice the cutoff set at $p = F$ and that the atom is most likely to be weakly coupled to the cavity.

We use equation (18) to create a distribution of atoms inside the cavity. Rempe *et al* [3] reported that for a random distribution of atom–field couplings with $C = \sum_j C_j$, A_ξ is modified in the following way:

$$1 + A_\xi = (1 + 2C)\frac{1 - \sum_j \frac{C_j'}{1+\sum_k C_k' - 2C_j'}}{1 + \left(1 + \frac{\gamma}{\kappa}\right)\sum_j \frac{C_j'}{1+\sum_k C_k' - 2C_j'}}. \tag{19}$$

Foster *et al* show in [1] an alternative, equivalent formulation of equation (19). Equation (19) reduces to (9) in the limit where all atoms are maximally coupled. It should also be stressed that equation (19) assumes that all the atoms are equally detuned which is clearly not the case for an atomic beam. We will treat all atoms resonantly. For a treatment of detunings, see [1].

We use equation (18) to evaluate the two sums in (19). The first sum over index k is the scaled-collective cooperativity parameter $\sum_j C_j/(1 + \gamma/2\kappa)$. Our approach is to couple an atom to the cavity according to equation (18) and repeat for N atoms. N is defined by the size of the interaction volume, V_F, and the density, ρ_{ab} of the atomic beam. The interaction volume is

$$V_F = \lambda_{\mathrm{c}} M w_0^2 \int_F^1 \frac{\cos^{-1}(p)}{p}\,\mathrm{d}p, \tag{20}$$

where M is the number of wavelengths of the cavity mode included in the mode volume and λ_{c} is the wavelength of the cavity light. The scaled cooperativity parameter becomes

$$\bar{C}' = \frac{\int_F^1 C_1' \frac{\cos^{-1}(p)}{p}\,\mathrm{d}p}{\int_F^1 \frac{\cos^{-1}(p)}{p}\,\mathrm{d}p} \times \rho_{\mathrm{ab}} V_F. \tag{21}$$

We know that for a homogeneously broadened cavity QED system, the collective cooperativity parameter is related to the experimentally accessible vacuum Rabi frequency $\bar{C} = \Omega^2/\kappa\gamma$. We use this fact along with equation (21) to obtain

$$\lambda_{\mathrm{c}}\rho_{\mathrm{ab}} M w_0^2 = \frac{8\Omega^2}{g^2\pi}. \tag{22}$$

The dependence on F has been removed and we can now set $F = 0$. As the volume extends to infinity, we include more atoms whose coupling approaches zero. We now evaluate the average of the sum over the index j in equation (19). Similarly to equation (21) we write

$$\overline{\sum} = \frac{\int_0^1 \frac{C_1'}{1+C'-2C_1'} \frac{\cos^{-1}(p)}{p}\,\mathrm{d}p}{\int_0^1 \frac{\cos^{-1}(p)}{p}\,\mathrm{d}p} \times \frac{8\Omega^2}{\pi g^2} \int_0^1 \frac{\cos^{-1}(p)}{p}\,\mathrm{d}p. \quad (23)$$

We can recast equation (23) into the following form:

$$\overline{\sum} = \frac{8\Omega^2}{2\pi g^2} \int_0^1 \frac{z\cos^{-1}(z)}{a^2 - z^2}\,\mathrm{d}z, \quad (24)$$

where

$$a^2 = \frac{\Omega^2 + \kappa\gamma\left(1 + \frac{\gamma}{2\kappa}\right)}{2g^2}. \quad (25)$$

We substitute the analytic form of equation (24) back into (19) to obtain an expression for the step in the field averaged over a random distribution of atoms:

$$1 + \overline{A_\xi} = (1 + 2C)\frac{1 + \frac{2C}{C_1}\ln\left(\frac{1}{2} + \frac{1}{2}\sqrt{1 - a^{-2}}\right)}{1 - (1 + \gamma/\kappa)\frac{2C}{C_1}\ln\left(\frac{1}{2} + \frac{1}{2}\sqrt{1 - a^{-2}}\right)}. \quad (26)$$

The overbar on A_ξ means we have averaged over the atomic distribution. Equation (26) provides a value for the initial fluctuation given a random distribution of atoms at rest. Notice that this function only requires the experimentally measurable values for g, κ, γ, and Ω.

We simplify equation (26) in the experimentally interesting limit of large atomic number where $C/C_1 \gg 1$

$$\overline{A_\xi} = -\tfrac{3}{4}C_1', \quad (27)$$

and the N identically coupled atom case in the same limit is

$$A_\xi = -2C_1'. \quad (28)$$

We find that, in the large beam density limit for a TEM_{00} Gaussian mode, the random distribution of atoms reduces the size of the field fluctuation by a factor of 3/8.

3.2. Homogeneous transit broadening

A thermal atomic beam degrades the size of quantum fluctuations through transit and Doppler broadening. We describe homogeneous transit broadening effects with the addition of a non-radiative homogeneous dephasing term to the system master equation (5) (see [22]),

$$\mathcal{L}_{\mathrm{dephase}}\rho = \tfrac{1}{2}\gamma_\mathrm{T}\sum_i(\sigma_z^i\rho\sigma_z^i - \rho) = \tfrac{1}{2}\gamma_\mathrm{T}\mathcal{D}[\sigma_z]\rho \quad (29)$$

where γ_T is equal to the average transit rate and is a function of the cavity waist and beam temperature. This addition to the master equation serves as a diffusive term that randomly flips the phase of the collective atomic polarization field. This approximates the effect of atoms leaving the cavity interaction region and modifies the radiative lifetime of the atoms in the following way: $\gamma \to \gamma' = \gamma + \gamma_\mathrm{T}/2$.

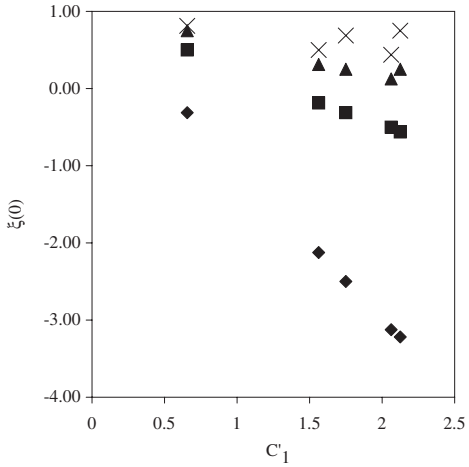

Figure 5. $\xi(0)$ as a function of C_1'. Crosses are from different experimental runs (see [1, 23, 24]). Filled symbols are calculations with varying degrees of corrections: diamonds are for N identically coupled atoms, squares are for N randomly coupled atoms from equation (26) with no transit broadening corrections, triangles include the homogeneous transit broadening described by equation (29).

3.3. Comparison with experiment

We have a large number of $g^{(2)}(\tau)$ measurements under different experimental conditions associated with our experiments in quantum feedback [23, 24]. Very briefly, a collimated beam of optically pre-pumped ^{85}Rb atoms interacts resonantly at the D_2 line (780 nm) with a single mode of a high finesse Fabry–Perot cavity. The cavity defines a TEM_{00} mode with two mirrors with different transmission coefficients, $T_1 = 15$ ppm and $T_2 = 300$ ppm. The input transmission is smaller than the output to ensure that most of the signal escapes from the cavity on the detector side. A typical cavity finesse for this arrangement is $\mathcal{F} \approx 21\,000$. We modify the coupling constant g by changing the separation (from 300 to 900 μm) and the radius of curvature (from 5 to 100 cm) of the mirrors to obtain ($3 < g < 12$). The reader can obtain complete experimental details in [1, 23, 24] that include our data taking procedure.

Figure 5 compares our measurements of the field step ξ from the correlation function $g^{(2)}(0)$, that characterize the sub-Poissonian statistics of the state of the electromagnetic field with the calculations from the model and its refinements from the previous sections. The measurements of $g^{(2)}(0)$ that we use to obtain $\xi(0)$ (crosses) typically have statistical errors of less than 5%. We start assuming N identically coupled atoms with the coupling constant g from the experiment and the vacuum Rabi frequency Ω set to match the experiment (diamonds). We then treat the atoms as N randomly coupled to the mode using equation (26) with g and Ω from the experiment. This brings the theoretical prediction (squares) closer. We finally treat transit broadening as a homogeneous process that modifies $\gamma/2\pi$ from 6.0 MHz to $\gamma'/2\pi = 9.2$ MHz (triangles). The agreement between experiment and theory gets better with each additional approximation. Further refinements would include inhomogeneous processes such as individual atomic detunings and transit times. These require a quantum Monte Carlo simulation. The agreement between our two corrections and

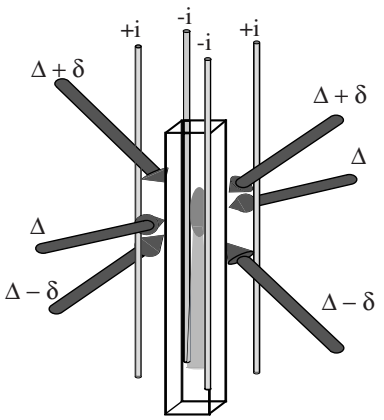

Figure 6. Sketch of a three-dimensional moving molasses setup. The up- and down-going beams are detuned from the cross-beam by δ. Four bars carry current I in opposite directions to create a quadrupole field in the horizontal plane.

the data suggests that we have a simple, analytical, approach for building cavities for observing the bouncing and cross-correlation effects.

4. Continuous cold beam

In order to reduce the effects that are limiting our measurements (see figure 5) we require a new source of atoms for future cavity QED experiments with the following constraints: the atoms should be continuous in order to maximize data-taking time. The atoms should be cold so as to reduce the Doppler and transit broadening effects, since both effects scale with the average velocity of the beam. The MOT trap beams should not overlap with the interaction volume of the cavity QED system to reduce background scattering. We also need to work with a relatively dense beam so that we typically have 50 or more atoms within the cavity volume at any given time, so reducing atom number fluctuation effects.

With these constraints in mind we review some of the previous work towards cold continuous atomic beams. Several groups have made progress by modifying the 3D MOT arrangement. Lu *et al* [25] loaded a 3D MOT from a background vapour and extracted atoms along one of the trap beams by unbalancing the power. Arlt *et al* [26] created pulsed cold atoms. They obtained typical atomic fluxes of 5×10^9 atoms s^{-1} with velocities around 7–20 m s^{-1} with a velocity spread of 2–3 m s^{-1} at FWHM. Weyers *et al* [27] employed a moving molasses technique to extract atoms along one of the trap beams.

The 2D MOT configuration makes the extraction process simpler. There is no magnetic confinement to overcome in the up–down direction. Berthoud *et al* [28] were able to extract atoms from this setup with a magnetic field applied along the z-axis. The flux of the beam in that setup, through a 1 cm diameter probe, was around 1.8×10^8 atoms s^{-1} with a velocity between 0.7 and 3.0 m s^{-1}. The magnetically extracted beam is complicated by the fact that it has three different velocity classes. The same group later modified their setup by switching to a moving molasses for extraction [5]. With the moving molasses they improved the beam flux by an order of magnitude and had a clean way of controlling the beam velocity.

We have a cold atom apparatus that follows [5]. Figure 6 shows the setup where four independent trap beams are detuned from each other in order to induce a drift velocity in the downward direction. The four current-carrying bars serve to create a 2D magnetic quadrupole field which traps the atoms in the x–y plane.

The (up-) down-going beams are detuned by (+)$-\delta$ from the overall detuning Δ. Typical values for δ range between 100 and 800 kHz. This detuning induces a drift velocity in the downward direction

$$v = \frac{\lambda\delta}{\cos\alpha} \tag{30}$$

where $\alpha = \pi/4$ is the angle that the up- and down-going beams make with the horizontal beam.

4.1. Experimental setup

Our system consists of a Coherent MBR110 Ti:sapphire laser. The output beam is split into a three beams for locking, trapping, and probing the atoms. We lock on to the $5S_{1/2}$, $F = 3 \rightarrow 5P_{3/2}$, $F = 4$ transition of ^{85}Rb at 780 nm with a saturation spectroscopy setup.

A New Focus Vortex laser serves to repump the atoms which fall out of the cycling transition and into the $5S_{1/2}$, $F = 2$ state. Another saturation spectroscopy setup provides the reference for locking this laser to the appropriate transition. The remaining power is mixed with the horizontal axis trap beam via a 1×2 single-mode fibre at 780 nm.

Independent control of the frequency of each trap beam is obtained by single-passing on-resonance light through an acousto-optical modulator (AOM) which downshifts the beam by 210 MHz. Three polarizing beamsplitters are then used to separate out each trap beam. They are double-passed through 80 MHz line centre AOMs and coupled into the trapping region with a standard circular polarization configuration. In order to achieve the detunings shown in figure 6, we independently launch the trap light from the fibre output couplers. The couplers create a clean Gaussian mode beam with diameter at $1/e^2$ of 8.7 mm. The power in each beam is approximately 3.1 mW. The horizontal axis beam is mixed with the repumper described above and retro-reflected.

The vacuum system pumps out both the trap cell and a lower chamber where the atomic beam is detected. The cell is optical quality quartz connected to a Pyrex glass tube attached to a high vacuum flange. An ion pump keeps the vacuum down to 1–2 $\times 10^{-8}$ Torr. At these pressures the trap $1/e$ lifetime is approximately 1 s. We introduce Rb atoms into the chamber by running a current through a Rb dispenser.

4.2. Results

We detect the cold atoms in two different ways: direct detection of the fluorescence onto a photomultiplier tube (PMT), and imaging with a charge coupled device (CCD) camera. The first detection system consists of a Hamamatsu R636 photomultiplier tube (PMT). A low noise current pre-amplifier from Stanford Research Systems SRS570 amplifies the signal from the PMT and we record it for further analysis with a Lecroy 9354A digital oscilloscope.

We load the trap for about 1 s, then as we shut off the trap beams, a shutter opens in front of the PMT. We collect

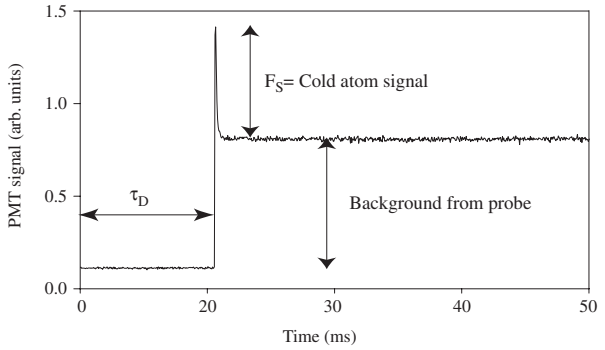

Figure 7. Fluorescence signal from the falling atoms F_S from a resonant laser probe 1 cm below the trap centre. The probe is turned on at τ_D about 20 ms after the trap light has been turned off.

the fluorescence from a resonant probe beam (≈80 ms) with an $f/3$ imaging system. The height of the probe and the PMT can be adjusted so that they are imaging up to 1 cm below the trap centre. We minimize room light background with a 780 interference filter in front of the PMT. Figure 7 shows a typical fluorescence signal F_S of ≈500 μs above the background from the atoms traversing the probe.

The large scatter from the uncoated cell makes it difficult to detect the atoms falling through the probe. We have found improvements in the signal-to-noise ratio if we wait until the atoms are in the centre of the probe area before turning on the probe. We use this technique of changing the delay between when the trap beams are shut off and when the probe is turned on in order to reconstruct the fall time of the cold atoms.

Figure 8(i) shows the fluorescence from cold atoms passing through the resonant probe located ≈7.5 mm below the trap centre after their release from the trap for a detuning of 100 KHz. The continuous line is a fit to a Gaussian. We repeat the measurement with four different detunings of 100, 200, 300, and 600 kHz. We fit each distribution and find the time location of the peak with uncertainties of less than 10%. Figure 8(ii) shows the measured peaks of the distributions for four different detunings. The continuous curve is the result of the calculation of the time evolution of the peak of the distribution from the kinematics of the cold atoms. We use equation (30) to find that the arrival times of the peak of the distributions correspond to velocities of 11, 22, 33, and 66 cm s^{-1}.

We use a CCD camera to collect the image from a probe region that is 25 cm below the trapping region in order to detect the continuous beam. The CCD camera allows us to take successive pictures with and without atoms to subtract resonant background. We integrate the signal over the entire visible probe area for both pictures and subtract one from the other to arrive at a signal normalized by the number of pixels included in the integration area. The results we report come from subtracting two large numbers. The beam-on and -off cases are 0.206 ± 0.036. This translates into a beam flux, through the probe, of $3.1 \pm 0.6 \times 10^4$ atoms s^{-1}.

The flux is small and at present will not be sufficient for conditional dynamics in cavity QED with many (≈50) atoms in the cavity. One drawback to the current setup is the size and shape of the glass cell used for trapping. Pumping the atoms into a dark state before exiting the trapping region should also significantly enhance the beam flux [29].

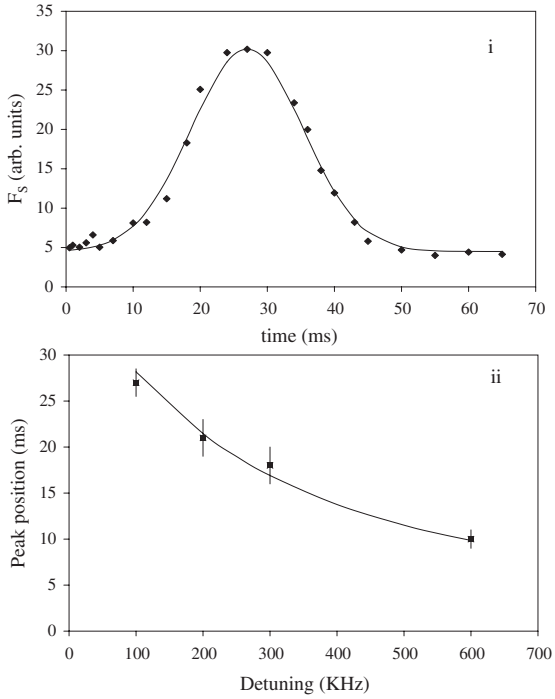

Figure 8. (i) F_S fluorescence signal from atoms passing the probe with detuning $\delta = 100$ kHz. The continuous curve is a Gaussian fit to the data. (ii) Peak of Gaussian distribution for four different detunings. The continuous curve is the calculation for the kinematics.

5. Conclusion

We have found expressions for the conditional dynamics of cavity QED in the presence of the random distribution of coupling constants brought by an atomic beam. The beam reduces the size of the non-classical effect, but does not destroy it. Other mechanisms that damage the fragile quantum state such as inhomogeneous broadening and transit broadening can decrease to acceptable levels with a cold atomic beam. We have presented our current realization of such a beam to continue measuring the conditional dynamics of cavity QED.

Acknowledgments

We would like to thank P Thomann and S Aubin for their interest and help with this project. Support for this project came from the NSF and NIST.

References

[1] Foster G T, Mielke S L and Orozco L A 2000 *Phys. Rev.* A **61** 053821
[2] Foster G T, Smith W P, Reiner J E and Orozco L A 2002 *Phys. Rev.* A **66** 033807
[3] Rempe G, Thompson R J, Brecha R J, Lee W D and Kimble H J 1991 *Phys. Rev. Lett.* **67** 1727
[4] Mielke S L, Foster G T and Orozco L A 1998 *Phys. Rev. Lett.* **80** 3948
[5] Berthoud P, Fretel E and Thomann P 1999 *Phys. Rev.* A **60** 4241
[6] Hood C J, Lynn R W, Doherty A C, Parkins A S and Kimble H J 2000 *Science* **287** 1447
[7] Pinkse P W H, Fischer T, Maunz P and Rempe G 2000 *Nature* **404** 365

[8] Guthohrlein G R, Keller M, Hayasaka K, Lange W and Walther H 2001 *Nature* **414** 49
[9] Mundt A B, Kreuter A, Becher C, Leibfried D, Eschner J, Schmidt-Kaler F and Blatt R 2002 *Phys. Rev. Lett.* **89** 103001
[10] McKeever J, Buck J R, Boozer A D, Kuzmich A, Nägerl H-C, Stamper-Kurn D M and Kimble H J 2003 *Phys. Rev. Lett.* **90** 133602
[11] Rice P and Leach J 2003 *Bull. Am. Phys. Soc.* **48-3** 85
[12] Adams C S, Sigel M and Mlynek J 1994 *Phys. Rep.* **240** 143
[13] Noh H R and Jhe W 2002 *Phys. Rep.* **372** 269
[14] Meschede D and Metcalf H 2003 *J. Phys. D: Appl. Phys.* **36** 17
[15] Berman P R (ed) 1994 Cavity quantum electrodynamics *Advances in Atomic, Molecular, and Optical Physics* (Suppl. 2) (Boston, MA: Academic)
[16] Carmichael H J 1993 *An Open Systems Approach to Quantum Optics* (*Springer Lecture Notes in Physics* vol 18) (Berlin: Springer)
[17] Reiner J E, Smith W P, Orozco L A, Carmichael H J and Rice P R 2001 *J. Opt. Soc. Am.* B **18** 1911
[18] Carmichael H J, Brecha R J and Rice P R 1991 *Opt. Commun.* **82** 73
[19] Lugiato L A 1984 *Progress in Optics* vol 21, ed E Wolf (Amsterdam: North-Holland) p 69
[20] Denisov A, Castro-Beltran H M and Carmichael H J 2002 *Phys. Rev. Lett.* **88** 243601
[21] Carmichael H J and Sanders B C 1999 *Phys. Rev.* A **60** 2497
[22] Clemens J P and Rice P R 2000 *Phys. Rev.* A **61** 063810
[23] Smith W P, Reiner J E, Orozco L A, Kuhr S and Wiseman H M 2002 *Phys. Rev. Lett.* **89** 133601
[24] Reiner J E, Smith W P and Orozco L A 2003 submitted
[25] Lu Z T, Corwin K L, Renn M J, Anderson M H, Cornell E A and Wieman C E 1996 *Phys. Rev. Lett.* **77** 3331
[26] Arlt J J, Marago O, Webster S, Hopkins S and Foot C J 1998 *Opt. Commun.* **157** 303
[27] Weyers S, Aucouturier E, Valentin C and Dimarcq N 1997 *Opt. Commun.* **143** 30
[28] Berthoud P, Joyet A, Dudle G, Sagna N and Thomann P 1998 *Europhys. Lett.* **41** 141
[29] Reitel G 2003 private communication